Sliding Extensive Cancellation Algorithm (ECA-S) for disturbance removal in passive radar

F. Colone, C. Palmarini, T. Martelli, E. Tilli

***Abstract*—In this paper an advanced version of the Extensive Cancellation Algorithm (ECA) is proposed for robust disturbance cancellation and target detection in passive radar. Firstly some specific limitations of previous ECA versions are identified when dealing with a highly time-varying disturbance scenario in the presence of slowly moving targets. Specifically, the need to rapidly adapt the filter coefficients is shown to yield undesired effects on low Doppler target echoes, along with the expected partial cancellation. Therefore a sliding version of the ECA is presented which operates on partially overlapped signal batches. The proposed modification to the original ECA is shown to appropriately counteract the limitations above by taking advantage of a smooth estimate of the filter coefficients. An efficient implementation is also discussed to limit the corresponding computational load. The benefits of the proposed approach are demonstrated against real data sets accounting for quite different passive radar applications.**

***Index Terms*— Passive radar, passive coherent location (PCL), disturbance removal, Extensive Cancellation Algorithm (ECA), adaptive filter.**

I. Introduction

In recent years Passive Coherent Location (PCL) has received a great interest for the potential role it could play in both civilian and military applications [1]-[3]. In fact the parasitic exploitation of an existing illuminator inherently implies a low environmental impact and a covert operation. In this regard PCL systems can be regarded as "invisible" systems catching extremely weak signals (target echoes) that are usually "invisible" to the ordinary users of the employed transmitter. This is made possible by the use of receivers with wide dynamic range and by the application of appropriate signal processing techniques to tackle the invisibility of such weak target echoes against typical undesired signal contributions, above all the direct signal breakthrough and multipath.

Indeed the disturbance cancellation represents one of the key stages within a conventional PCL processing scheme. In particular, when the PCL is equipped with a single or few receiving channels, this task is usually accomplished in the time domain. To this purpose, the signal collected at the reference channel is typically exploited to remove undesired contributions, received together with the moving target echo, on the surveillance channel. Different approaches have been proposed to cope with this problem yielding solutions with different complexity and effectiveness [4]-[18].

Among these approaches, a widely used cancellation technique is the Extensive Cancellation Algorithm (ECA) and its Batches version (ECA-B) [13]. The ECA basically operates by subtracting, from the surveillance signal, delayed replicas of the reference signal properly weighted according to adaptively estimated coefficients. In its original version, the ECA requires the filter weights to be estimated by averaging over the whole coherent processing interval (CPI).

In contrast, the ECA-B approach estimates and applies the filter weights over smaller portions (batches) of the integration time. Reducing the temporal dimension of the single batch within certain limits does not yield significant adaptivity loss when operating in a stationary environment. However, the ECA-B was demonstrated in [13] to make the system more robust to the time-varying characteristics of the environment; this has been shown to be an appreciable advantage in many applications, especially when operating against non-stationary disturbance scenarios.

The techniques above have been largely employed by the authors as well as by other research groups and became a key-step within the signal processing chain of many different PCL prototypes. A number of contributions appeared in the open literature where the effectiveness of these cancellation approaches has been clearly demonstrated with reference to quite different PCL applications exploiting various waveforms of opportunity, e.g. [18]-[35].

Nevertheless, in this paper we show that the ECA-B might yield some limitations when employed against highly time-varying disturbance scenarios in the presence of slowly moving targets. In fact the need for a rapid update of filter coefficients contrasts with the necessity to preserve the slowly moving target echo. In other words, using short batches widens the cancellation filter notch in the Doppler dimension yielding to a partial cancellation of the target return. Along with this obvious effect, we show that the batches operation yields undesired effects on the target echo at the output of the cancellation stage; such effects are then responsible for the emergence of unwanted structures in the range-Doppler map obtained at the output of the 2D cross-correlation between the reference and the surveillance signals.

Aiming at counteracting these limitations, we introduce a

F. Colone, C. Palmarini, and T. Martelli are with the DIET Department, University of Rome "La Sapienza," Via Eudossiana, 18 – 00184 Rome, Italy (e-mail: {colone, palmarini, martelli}@diet.uniroma1.it).

E. Tilli is with Selex-ES a Finmeccanica company, Via Tiburtina km 12400 – 00131 Rome, Italy (e-mail: enrico.tilli@selex-es.com).

modified version of the ECA-B that operates over partially overlapped portions of the received signals. This ECA-Sliding (ECA-S) approach allows to separately set the update rate of the filter coefficients and the batch duration exploited for the adaptive estimation of the coefficients themselves. Therefore a better cancellation capability can be achieved by performing a rapid enough update of the filter weights; however the latter are obtained from longer and partially overlapped signal fragments in order to guarantee an accurate and smoothed estimation of the disturbance characteristics.

Obviously this is paid in terms of computational load since the number of complex operations to be performed increases with the percentage of overlap between successively processed signal fragments. Therefore we discuss some expedients to enable an efficient implementation of the proposed approach. These expedients have a more general value as they can be fruitfully adopted to limit also the computational burden of the previous ECA versions.

The advantages yield by the proposed ECA-S approach are verified in this paper with reference to three live data sets accounting for very different PCL applications. Specifically a WiFi-based PCL is considered for target detection at short range aiming at local area surveillance. A DVBT-based PCL is exploited for medium range maritime surveillance. Finally an FM-based PCL is employed for typical air traffic control (ATC) applications.

The paper is organized as follows. The ECA and the ECA-B approaches are briefly recalled in Section II and some real-life examples are shown to demonstrate the benefits of a batches operation in different surveillance applications. The limitations of the ECA-B are investigated in Section III by means of theoretical derivations and experimental results. Then the ECA-S approach is presented in Section IV and its effectiveness is demonstrated in Section V against real data sets compared to previous ECA versions. Section VI reports some considerations on the computational load aiming at the practical implementation of the proposed approach. Finally our conclusions are drawn in Section VII.

II. The ECA and ECA-Batches approaches

As well known the ECA operates by subtracting from the surveillance signal $s_s(t)$ properly scaled and delayed replicas of the reference signal $s_r(t)$ [13]. Specifically, by sampling the received signals at f_s and assuming that the multipath echoes are backscattered from the first K range bins, the output of the ECA is evaluated as:

$$s_{ECA}[n] = s_s[n] - \sum_{k=0}^{K-1} \alpha_k s_r[n-k] \quad n = 0, \dots, N-1 \quad (1)$$

being N the number of samples within the CPI T_{int}. The filter coefficients $\boldsymbol{\alpha} = [\alpha_0 \ \alpha_1 \ \cdots \ \alpha_{K-1}]^{\boldsymbol{T}}$ are evaluated by resorting to a Least Square (LS) approach that minimizes the power of the signal at the output of the filter:

$$\boldsymbol{\alpha} = (\mathbf{S}_r^{\mathrm{H}}\mathbf{S}_r)^{-1}\mathbf{S}_r^{\mathrm{H}}\mathbf{s}_s \quad (2)$$

where $\mathbf{s}_s$ is a $N \times 1$ vector containing N samples of the surveillance signal and $\mathbf{S}_r$ is a $N \times K$ matrix whose columns are the delayed versions of the reference signal. As is apparent, in its original version, the ECA requires the filter weights to be estimated over the whole CPI.

In contrast, the ECA-B output at the l-th batch is written as

$$s_{ECA-B}[n] = s_s[n] - \sum_{\mathrm{k}=0}^{\mathrm{K}-1} \alpha_k^{(l)} s_r[n-k]$$

$$n = lN_B, \dots, (l+1)N_B - 1; \ l = 0, \dots, B-1 \quad (3)$$

where N_B is the dimension of each batch, $B = \left\lfloor \frac{N}{N_B} \right\rfloor$ is the number of batches, and $\boldsymbol{\alpha}^{(l)} = \left[\alpha_0^{(l)} \ \alpha_1^{(l)} \ \cdots \ \alpha_{K-1}^{(l)}\right]^T$ is the filter coefficients estimate obtained at the l-th batch, namely by exploiting the l-th signal fragment of duration $T_B = N_B/f_s$. Basically we have

$$\boldsymbol{\alpha}^{(l)} = \left[\mathbf{S}_r^{(l)^H}\mathbf{S}_r^{(l)}\right]^{-1}\mathbf{S}_r^{(l)^H}\mathbf{s}_s^{(l)} \quad (4)$$

where $\mathbf{s}_s^{(l)} = \left[s_s[lN_B], \ s_s[lN_B+1], \cdots, s_s[(l+1)N_B-1]\right]^T$ is a $(N_B \times 1)$ vector and $\mathbf{S}_r^{(l)}$ is a $N_B \times K$ matrix collecting the delayed copies of the corresponding reference signal fragment. The ECA-B has been demonstrated to yield effective disturbance cancellation and target detection in a number of applications [13], [29]-[35]. Usually the batch duration T_B has to be carefully selected as it affects the capability of the system to adapt to the time-varying characteristics of the environment. However, to avoid undesired effects, the need for a rapid update of filter coefficients has to be traded with the accuracy of the adaptive estimation and with the necessity of preserving the target echo.

These points are investigated here with reference to quite different PCL applications by exploiting real data sets collected in various conditions. Specifically three PCL experimental prototypes have been used that exploit different waveforms of opportunity and are intended for various surveillance applications.

A. FM-based PCL for ATC applications

First of all we consider a long range surveillance application using the FM radio signal as waveform of opportunity. Specifically we exploit the data set collected on June 7th 2012, in a site near the Fiumicino Airport of Rome. Receiver architecture and acquisition geometry are described in detail in [29]. Enough to know that two antennas were used: one antenna was employed to collect the reference signal and was steered toward the transmitter located on Monte Cavo, about 35 km South-East of the receiver site; the other antenna was pointed toward the opposite direction to gather the surveillance signal. Several sequential data acquisitions were performed for different FM radio channels; each data file is about 1.1 sec of duration, with a temporal spacing of about 2.3 sec between two consecutive acquisitions. All the available data files have been first processed according to different ECA versions with K=140 taps (i.e. 210 km @ f_s=200 kHz).

The disturbance cancellation capability is studied in Figure 1 along 200 consecutive data files for different choices of the batch duration employed by the ECA-B. The reported clutter attenuation (CA) is defined as the ratio between the power levels measured, over the considered FM radio channel bandwidth, at the input and at the output of the cancellation filter. As is apparent, operating with a conventional ECA (i.e. $T_B = 1$ s in this application where $T_{int} = 1$ s is adopted) yields a significant cancellation loss with respect to the theoretical cancellation (about 52 dB); this can be attributed to a number of factors there including Tx/Rx non-idealities as well as the presence of interference. Nevertheless, disturbance removal via ECA-B provides remarkably better results making the system robust to slowly varying conditions of the observed scenario. Specifically reducing the batch duration down to $T_B = 25$ ms allows a significant improvement in term of CA with respect to the conventional ECA. In fact the average CA increases by 6 dB and the performance is much more stable along the acquisition time. Further reducing the batch duration might yield some degradation in most of the considered data files due to the progressively larger adaptivity loss. Therefore T_B values around 25 ms will be considered in the following to guarantee effective cancellation against this specific scenario.

B. DVBT-based PCL for maritime surveillance

Due to their fine range resolution and the high effective radiated power (ERP) associated with their illuminators, Digital Video Broadcasting-Terrestrial (DVB-T) transmissions represent one of the most attractive choices to be used for naval target localization and tracking. The potentialities of DVB-T based PCL have been preliminary demonstrated both for short/medium [36] and for long range maritime surveillance [37].

Here we report the results obtained against the DVB-T based PCL data collected during the acquisition campaigns held by Selex-ES at various sites along the Italian coastline. In Figure 2 we focus on four different data sets; for each of them 30 consecutive data files of duration 1 s have been considered and ECA-B with different values of batch duration, T_B, has been applied to the received signals. Since a CPI of 1 s is adopted in the following, setting $T_B = 1$ s corresponds to the application of ECA. In particular, the CA as a function of T_B is reported in Figure 2, averaged over the considered 30 data files for each considered Data Set.

As is apparent, Data Sets 1 and 2 account for quite stationary scenarios. In this case an almost flat trend of CA is observed for high enough values of the batch duration (i.e. $T_B > 0.1$ s); further decreasing the batch duration leads to an increase of the adaptivity loss thus yielding slightly worse disturbance cancellation.

In contrast, when the system operates against highly non-stationary scenarios, progressive decrease of T_B allows to better adapt to the varying characteristics of the disturbance (see Data Sets 3 and 4). However it is worth noticing that uncontrolled decrease of the batch duration may lead to detrimental detection losses for slowly moving targets that fall in the cancellation filter. For this reason, it is convenient to identify a useful set of T_B values that: (i) give rise to small CA losses when working in stationary scenarios and (ii) yield a good trade-off between measured CA and slowly moving targets detection when

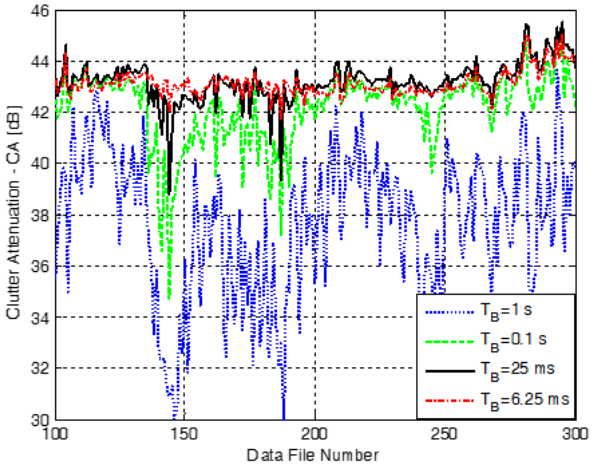

Figure 2. Clutter attenuation (CA) along the acquisition for the ECA-B operating with different batch durations.

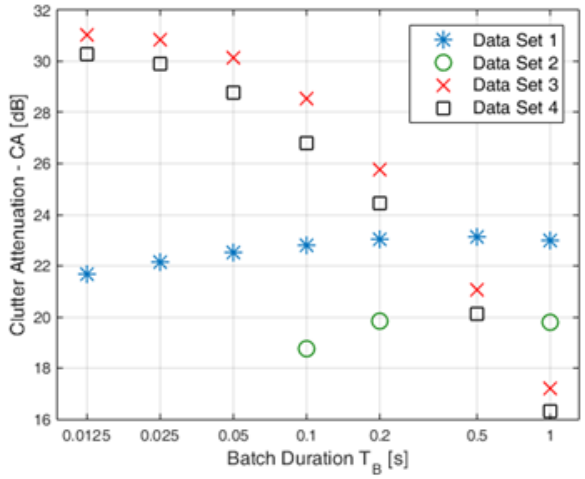

Figure 1. Clutter attenuation (CA) as a function of the batch duration for the ECA-B. Comparison between data sets acquired in different scenarios.

dealing with non-stationary scenarios. Based on the analysis reported in Figure 2, a reasonable choice could be $T_B \in [0.05\text{ s}, 0.2\text{ s}]$.

C. WiFi-based PCL for local area monitoring

WiFi transmissions might be successfully exploited in local area monitoring applications aiming at the detection of designated vehicles or human beings within public/private buildings and surrounding areas [34]-[35]. As an example of this application, we show the results obtained using the experimental equipment described in [35]. In particular, a wireless access point (AP) was employed, set up to emit the beacon signal at 3 ms, and a quasi monostatic configuration was adopted for the surveillance and the transmitting antennas. Tests have been performed in a parking area using vehicles as cooperative targets.

In addition, in this specific application we were allowed to perform some target-free tests in order to evaluate the disturbance cancellation capability in controlled situations avoiding the target effects. To this purpose, an acquisition of 20 s is considered in the following that includes just disturbance

contributions (direct signal and echoes from the stationary scene).

Figure 3 reports the cancellation performance along the acquisition time for the ECA-B operating over a range extension of 500 m with different durations of the batch. In this application, the measured CA is close to the maximum theoretical expected value (29.4 dB) even operating with long batches (i.e. using a conventional ECA). In fact in this case, the system operates in a scenario that mostly includes man-made objects. Therefore the non-stationary behavior of the received signals is mostly due to the instabilities of both the transmitter and the receiver. Nevertheless the decrease of the batch duration allows a slight improvement in term of average CA: about 0.4 dB gain is obtained moving from $T_B = 0.5$ s to $T_B = 15$ ms (Figure 3(a) and Figure 3(d), respectively). Moreover we observe that a much more stable CA is achieved along the acquisition time which clearly demonstrates the increased capability to adapt to the time-varying characteristics of the collected signals.

This analysis allows us to select a batch duration between 50 ms and 15 ms. Notice that, in this case it is not recommended to further decrease T_B since we recall that WiFi transmissions are of a pulsed type and, due to the exploited Carrier Sense Multiple Access (CSMA) approach, the transmission may be inhibited for a long time thus yielding a high temporal separation among consecutive pulses. Therefore operating with very small batches there might be a high variability in the number of pulses included in each batch and, in extreme cases, this might yield empty batches.

III. Limitations of the ECA-B

The benefits of the ECA-B approach have been shown in the previous section in term of disturbance cancellation capability. Specifically, it has been verified that, widening the cancellation notch by reducing the batch duration up to a certain limit allows a better removal of the disturbance contributions.

Obviously, this has a non negligible impact on the target echoes, especially those observed at low Doppler frequencies. However, we show that this impact is not limited only to the typical SNR loss due to the partial cancellation of slowly moving target echoes.

To this purpose we consider the two-dimensional (range-Doppler) cross-correlation between the reference signal and the surveillance signal after the disturbance cancellation stage. The resulting map is a representation of the range-Doppler distribution of the signal energy at the output of the cancellation filter. Therefore its analysis gives a further insight into the performance of the considered cancellation algorithm.

For example, let us consider the short range application employing a WiFi-based PCL, in which it is quite typical to deal with targets observed at low Doppler frequency, namely slowly-moving targets or targets moving mainly along the cross-range direction. Therefore it is of interest to study the effect of the ECA-B on the detection of such targets. To this purpose we show the results obtained with the experimental set-up described in Section II.C, for a test performed against a

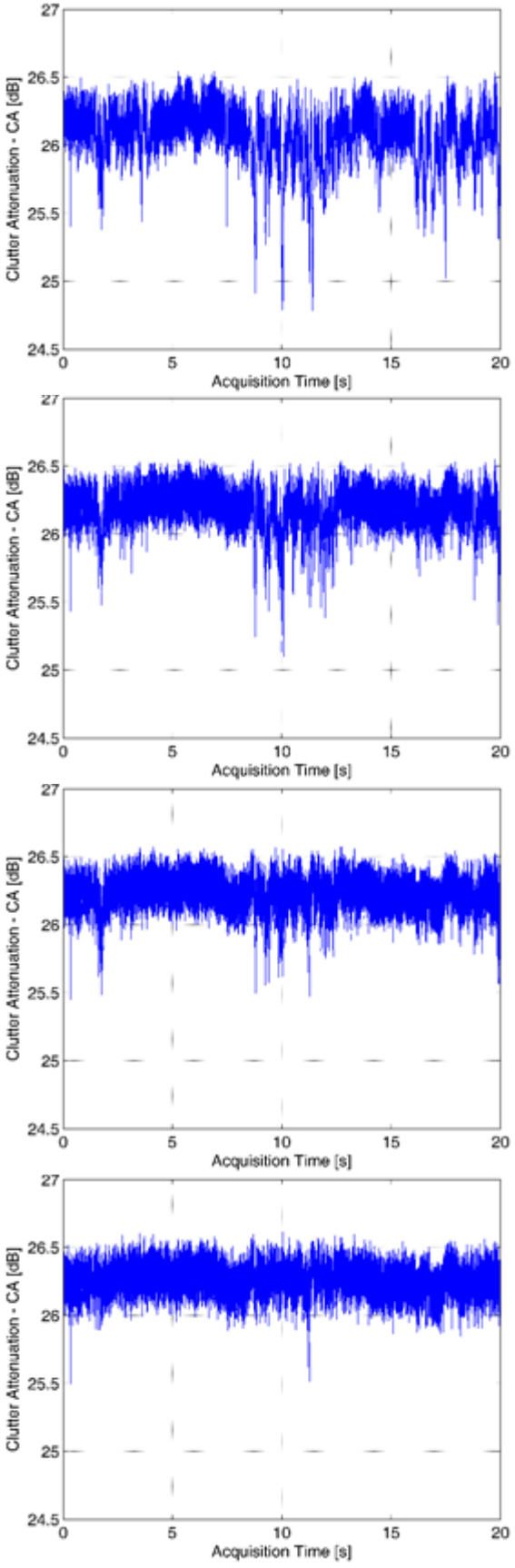

Figure 3. Clutter attenuation (CA) along the acquisition time for the ECA-B operating with different batch durations. (a) $T_B = 0.5$ s; (b) $T_B = 0.1$ s; (c) $T_B = 50$ ms; (d) $T_B = 15$ ms.

vehicular target moving in the cross-range direction with approximate speed 4.5 m/s and distance of minimum approach R_0 = 20 m. In such geometry, the target describes a parabolic trajectory on the bistatic range-Doppler plane and, for a long time, it will be observed at Doppler frequencies within or close to the cancellation filter notch. As an example, Figure 4 and Figure 5 show the range-Doppler maps obtained after disturbance cancellation with a CPI $T_{int} = 0.2$ s for two different positions of the target along its trajectory. Proper techniques have been applied to control the sidelobes level of the signal ambiguity function [34]. All the reported maps have been normalized to thermal noise power level so that the value at each map location represents the estimated signal to noise ratio (SNR). Notice that the dynamic range has been lower limited to better highlight the main structures arising in the map. The adopted cancellation filters operate over a range extension of 500 m with different values of the batch duration T_B.

Specifically, Figure 4 accounts for a favorable situation since the target Doppler frequency is reasonably high so that it is not affected by the cancellation stage. In fact, in this case, the ECA-B operates with $T_B = 50$ ms that yields a notch Doppler extension equal to approximately $1/T_B$ which is significantly smaller than the target Doppler value. As a consequence, after the cancellation stage, the target appears as a strong peak at 53 m and -41 Hz. In addition, a further peak is also visible at 161 m and -33 Hz caused by the double-bounce reflection of the target echo over the metallic fence delimiting the parking area.

In contrast, Figure 5 shows the case of a target echo included in the filter notch so that it is expected to be strongly affected by the cancellation stage. In particular, Figure 5(a-c) have been obtained by using batch durations equal to $T_B = 50$ ms, $T_B = 30$ ms, and $T_B = 15$ ms, respectively.

As is apparent, in all cases, the target peak is surrounded by undesired structures in the Doppler dimension that might be responsible of useful dynamic range reduction or masking effects over weak targets, thus limiting the detection capability. These Doppler ambiguities are mainly due to the ECA-B approach that exploits consecutive batches of the received signals where the filter coefficients are separately estimated and applied. In fact this yields discontinuities in the target echo at the output of this stage appearing at regular intervals of T_B thus setting the Doppler spacing between unwanted peaks ($1/T_B$).

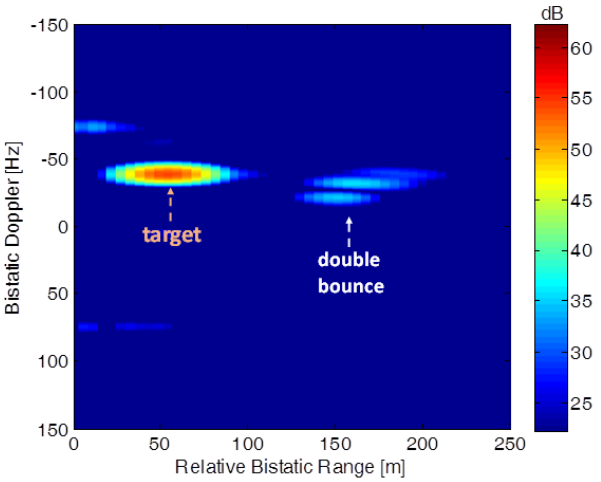

Figure 4. Range-Doppler map after ECA-B with $T_B = 50$ ms in the case of a high Doppler target.

This is demonstrated here with reference to the following simplifying hypotheses:

(i) the surveillance signal includes a single moving target echo observed with amplitude A_t at Doppler f_d with delay $\tau = n_\tau/f_s$, a single zero-Doppler replica of the transmitted signal received from the same target range cell (i.e. delay τ) with amplitude A_c, and thermal noise w_s:

$$s_s[n] = A_t d[n - n_\tau] e^{j2\pi f_d n/f_s} + A_c d[n - n_\tau] + w_s[n]$$
$$n = 0, \dots, N-1 \qquad (5)$$

where $d[n]$ is the signal emitted by the illuminator of opportunity with unitary average power. Notice that the zero-Doppler term in (5) might represent either the direct signal from the transmitter or a stationary multipath contribution.

(ii) The reference signal is an ideal noise-free copy of the transmitted signal: $s_r[n] = A_r d[n]$, $n = 0, \dots, N-1$.

(iii) The ECA filter operates with a single tap, i.e. $K = 1$, against the sole range cell at delay τ that includes both the target and the multipath echoes. Without loss of generality we further assume that $\tau = n_\tau/f_s = 0$.

With the positions above, the filter in (*2*) and (4) reduces to a single complex coefficient. In particular, at the *l*-th batch ($l = 0, \dots, \left\lfloor \frac{N}{N_B} \right\rfloor - 1$), it can be written as:

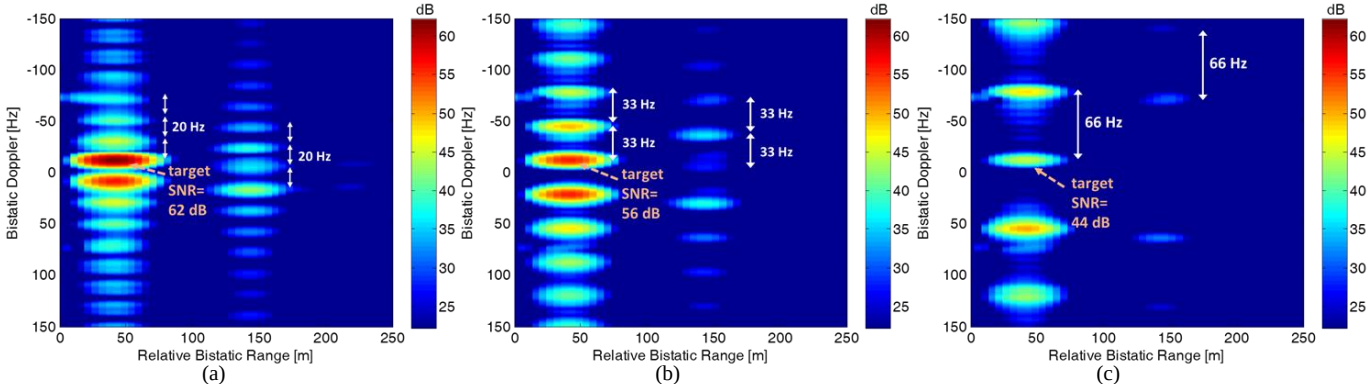

Figure 5. Range-Doppler maps after ECA-B for three different batch durations in the case of a low Doppler target: (a) $T_B = 50$ ms; (b) $T_B = 30$ ms; (c) $T_B = 15$ ms

$$\alpha_0^{(l)} = \frac{1}{\left\|\mathbf{s}_r^{(l)}\right\|^2}\mathbf{s}_r^{(l)^H}\mathbf{s}_s^{(l)} =$$

$$= \frac{1}{|A_r|^2\|\mathbf{d}^{(l)}\|^2}\left[A_r^* A_t \mathbf{d}^{(l)^H}\mathbf{d}_{f_d}^{(l)} + A_r^* A_c\left\|\mathbf{d}^{(l)}\right\|^2 + \right.$$

$$\left. + A_r^* \mathbf{d}^{(l)^H}\mathbf{w}_s{}^{(l)}\right] \quad (6)$$

where $\mathbf{d}^{(l)}$ is the $N_B \times 1$ vector containing the l-th batch of the direct signal and $\mathbf{d}_{f_d}^{(l)}$ is its Doppler shifted version.

Consequently, the output of the ECA-B at the l-th batch is:

$$\mathbf{s}_{ECA-B}^{(l)} = \mathbf{s}_s^{(l)} - \alpha_0^{(l)}\mathbf{s}_r^{(l)} =$$

$$= A_t\mathbf{d}_{f_d}^{(l)} - \frac{A_t}{\|\boldsymbol{d}^{(l)}\|^2}\mathbf{d}^{(l)^H}\mathbf{d}_{f_d}^{(l)}\mathbf{d}^{(l)} + \mathbf{w}_s{}^{(l)} +$$

$$- \frac{1}{\|\mathbf{d}^{(l)}\|^2}\mathbf{d}^{(l)^H}\mathbf{w}_s{}^{(l)}\mathbf{d}^{(l)} \quad (7)$$

where the original stationary disturbance contribution in the surveillance signal has been perfectly removed thanks to the simplifying hypotheses above. As is apparent the ECA-B output includes the ideal target contribution, $A_t\mathbf{d}_{f_d}^{(l)}$, along with an additional zero-Doppler contribution whose amplitude depends both on the target amplitude A_t and on the target Doppler frequency via the scalar product $\mathbf{d}^{(l)^H}\mathbf{d}_{f_d}^{(l)}$. Therefore this term cannot be neglected for slowly moving target echoes, i.e. targets observed at low Doppler frequencies, and it encodes the partial removal of the target echo due to the application of the cancellation filter. Similarly, the original thermal noise contribution, $\boldsymbol{w}_s{}^{(l)}$, is present together with a noise-dependent term which yields the theoretical upper bound to the achievable cancellation of zero-Doppler contributions.

To better understand the impact of the different contributions in **Errore. L'origine riferimento non è stata trovata.**, we can evaluate the output of the range-Doppler map $\chi[\tau_0, f_0]$ at the generic delay-Doppler bin (τ_0, f_0) where the presence of targets is sought. Specifically, based on the observation that the undesired structures due to the ECA-B application appear in the Doppler dimension (see **Errore. L'origine riferimento non è stata trovata.**), we focus on the range bin containing the target echo, i.e. $\tau_0 = \tau = 0$. Therefore, to simplify the mathematical notation, we define $\bar{\chi}\left[f_0\right] = \chi\left[\tau = 0, f_0\right]$. This can be evaluated as:

$$\bar{\chi}[f_0] = \mathbf{d}_{f_0}^H\mathbf{s}_{ECA-B} =$$

$$= \mathbf{d}_{f_0}^H\begin{bmatrix}\mathbf{s}_{ECA-B}^0 \\ \vdots \\ \mathbf{s}_{ECA-B}^{B-1}\end{bmatrix} = \sum_{l=0}^{B-1}\mathbf{d}_{f_0}^{(l)^H}\mathbf{s}_{ECA-B}^{(l)} \quad (8)$$

Substituting (7) into (8) we obtain:

$$\bar{\chi}[f_0] = \sum_{l=0}^{B-1} A_t\mathbf{d}_{f_0}^{(l)^H}\mathbf{d}_{f_d}^{(l)} - \sum_{l=0}^{B-1}\frac{A_t}{\|\mathbf{d}^{(l)}\|^2}\mathbf{d}^{(l)^H}\mathbf{d}_{f_d}^{(l)}\mathbf{d}_{f_0}^{(l)^H}\mathbf{d}^{(l)} +$$

$$+ \sum_{l=0}^{B-1}\left[\mathbf{d}_{f_0}^{(l)^H} - \frac{1}{\|\mathbf{d}^{(l)}\|^2}\mathbf{d}_{f_0}^{(l)^H}\mathbf{d}^{(l)}\mathbf{d}^{(l)^H}\right]\mathbf{w}_s{}^{(l)} \quad (9)$$

Aiming at understanding the impact of the ECA-B on the target echo, we focus our attention on the first two terms in eq. (9). Specifically, for the first term we might write:

$$\bar{\chi}_I[f_0] = \sum_{l=0}^{B-1} A_t\mathbf{d}_{f_0}^{(l)^H}\mathbf{d}_{f_d}^{(l)} = A_t\mathbf{d}_{f_0}^H\mathbf{d}_{f_d} =$$

$$= A_t\sum_{n=0}^{N-1}|d[n]|^2\, e^{-j2\pi(f_0 - f_d)n/f_s} \quad (10)$$

This term represents the ideal target contribution at the output of the 2D-CCF and its shape in the Doppler dimension strongly depends on the signal ambiguity function. As expected, for a constant modulus signal, eq. (10) yields the typical $\sin(Nx)/\sin(x)$ shape centered in $f_0 = f_d$ with peak amplitude $A_t N$, main lobe width $f_s/N = 1/T_{int}$, and period f_s:

$$\bar{\chi}_I[f_0] = A_t\frac{sin[\pi(f_d - f_0)\,N/f_s]}{sin[\pi(f_d - f_0)/f_s]}e^{j\pi(f_d - f_0)(N-1)/f_s} \quad (11)$$

The second term in eq. (9) can be written as:

$$\bar{\chi}_{II}[f_0] = A_t N_B^2\sum_{l=0}^{B-1}\frac{1}{\|\boldsymbol{d}^{(l)}\|^2}g^{(l)}(f_d)\left[g^{(l)}(f_0)\right]^* \quad (12)$$

where $g^{(l)}(f) = \mathbf{d}^{(l)^H}\mathbf{d}_f^{(l)}/N_B$ is the output of the zero-Doppler filter for a unitary input signal with Doppler shift f. Notice that, for a constant amplitude signal, it results

$$g^{(l)}(f) = \frac{1}{N_B}\sum_{n=lN_B}^{(l+1)N_B-1}|d[n]|^2\, e^{j2\pi fn/f_s} =$$

$$= g^{(0)}(f)e^{j2\pi flN_B/f_s} \quad (13)$$

being

$$g^{(0)}(f) = \frac{1}{N_B}\sum_{n=0}^{N_B-1} e^{j2\pi fn/f_s} =$$

$$= \frac{1}{N_B}\frac{sin[\pi f N_B/f_s]}{sin[\pi f/f_s]}e^{j\pi f(N_B-1)/f_s} \quad (14)$$

and eq. (12) becomes:

$$\bar{\chi}_{II}[f_0] = A_t N_B g^{(0)}(f_d)\left[g^{(0)}(f_0)\right]^*\sum_{l=0}^{B-1} e^{j2\pi(f_d - f_0)lN_B/f_s} =$$

$$= A_t N_B g^{(0)}(f_d)\left[g^{(0)}(f_0)\right]^*\frac{sin[\pi(f_d - f_0)\,BN_B/f_s]}{sin[\pi(f_d - f_0)N_B/f_s]}\cdot$$

$$\cdot\, e^{j\pi(f_d - f_0)(B-1)N_B/f_s} \quad (15)$$

As is apparent $\bar{\chi}_{II}[f_0]$ includes a $\sin(Bx)/\sin(x)$ shaped factor centered in $f_0 = f_d$ with period $f_s/N_B = 1/T_B$. Notice that its main lobe width coincides with that in eq. (11) whereas its peak amplitude is modulated by the product $G(f_d, f_0) = g^{(0)}(f_d)\left[g^{(0)}(f_0)\right]^*$ which separately depends on the target

Doppler frequency f_d and the Doppler of interest f_0 and we have $|G(f_d, f_0)| \leq 1$.

Let us consider the global output at specific Doppler values. Setting $f_0 = f_d$ we infer that the target peak value is subject to a loss due to the cancellation stage. In fact in this case we obtain:

$$\bar{\chi}[f_d] = \bar{\chi}_I[f_d] - \bar{\chi}_{II}[f_d] = \\ = A_t N \left\{ 1 - \left| \frac{1}{N_B} \frac{sin[\pi f_d N_B / f_s]}{sin[\pi f_d / f_s]} \right|^2 \right\} \quad (16)$$

As expected, for a given batch duration, the loss depends on the target Doppler frequency and cannot be neglected as far as $|f_d| < 1/T_{\mathrm{B}}$.

It is interesting to evaluate the output at the ambiguous peaks of the $\sin(Bx)/\sin(x)$ term in (15), i.e. for $|f_0 - f_d| = \frac{p}{T_{\mathrm{B}}} (p \in \mathbb{Z}, p \neq 0)$. First of all we observe that this condition does not guarantee that both f_0 and f_d are multiples of $\frac{1}{T_{\mathrm{B}}}$, so that in the general case $G(f_d, f_0) \neq 0$ and the Doppler ambiguities clearly appear in the final map:

$$\left| \bar{\chi} \left[f_d + \frac{p}{T_{\mathrm{B}}} \right] \right| = \\ = \left| A_t \frac{N}{N_B^2} \frac{sin[\pi f_d N_B / f_s]}{sin[\pi f_d / f_s]} \frac{sin\left[\pi (f_d + \frac{p}{T_{\mathrm{B}}}) N_B / f_s\right]}{sin\left[\pi (f_d + \frac{p}{T_{\mathrm{B}}}) / f_s\right]} \right| \quad (17)$$

For a slowly moving target included in the cancellation notch, i.e. $|f_d| < 1/T_{\mathrm{B}}$, the first $sin[N_B \mathrm{x}]/sin[x]$ factor has non negligible values while the amplitude of the second factor decreases as $|p|$ increases. Therefore, in such conditions the target response at the output of the 2D-CCF map shows Doppler ambiguities separated by $1/T_{\mathrm{B}}$ with amplitudes decaying at high Doppler frequencies.

This is clearly the case observed in Figure 5. Notice that as the batch duration decreases, the Doppler ambiguities spread accordingly. In addition, the cancellation notch is widened and the target SNR is progressively reduced. Further decreasing T_B would allow the undesired structures to be moved out of the Doppler range of interest. However this would also yield a more severe slowly-moving target removal and additional adaptivity loss since the disturbance characteristics would be estimated on few signal samples.

The above limitation of the ECA-B is apparent in PCL local area applications where it is quite typical to deal with slowly moving targets. However, similar effects can be observed also in longer range applications, especially when exploiting signals of opportunity in the VHF or UHF band since there is a reasonable probability to observe a target at low Doppler frequency. This certainly applies to the maritime surveillance application where small boats or docked vessels might show very limited velocities. However, even in ATC applications, targets could be present moving mainly along the cross-range direction.

These considerations exacerbate in severe scenarios (i.e. those characterized by rapidly varying disturbance characteristics, possibly induced by co- and inter-channel interference, severe multipath, transmitter dependent effects, etc.) where it may be necessary to frequently update the filter coefficients to effectively remove the disturbance. In fact, operating with the ECA-B this is tantamount to the request for batches of extremely small dimension. Unluckily, this results in a considerable widening of the cancellation filter notch thus including even fast moving targets.

IV. The ECA-Sliding technique

Based on the previous analysis, when the ECA-B approach is applied, special attention should be devoted to the selection of the batch duration as it affects both the capability to effectively remove the disturbance contributions possibly showing a non-stationary behavior and the possibility to nicely preserve the target echo.

Specifically the two requirements above might set opposite constraints on the selection of T_B. Long T_B should be selected to reduce the minimum detectable velocity and to limit the adaptivity loss. In contrast, short T_B should be preferred to be effective against disturbance with rapidly varying characteristics and to move the target Doppler ambiguities out of the observed Doppler extent.

To overcome this limitation, we propose a sliding version of the ECA (ECA-S) which operates over partially overlapped signal fragments (see Figure 6). This allows to decouple the selection of the batch duration exploited for the filter estimation and the update rate of the filter coefficients so that the requirements above could be more flexibly traded for.

Basically a new parameter is introduced, T_S, that represents the signal fragment processed using a given filter estimate; apparently, T_S also coincides with the temporal separation between consecutive updates of the filter coefficients. Thus ECA-S output at the *l*-th fragment is written as

$$s_{ECA-S}[n] = s_s[n] - \sum_{k=0}^{K-1} \alpha_k^{(l,T_A)} s_r[n-k] \\ n = lN_S, \ldots, (l+1)N_S - 1;\ l = 0, \ldots, B_S - 1 \quad (18)$$

where N_S is the dimension of each fragment (i.e. $N_S = T_S f_s$), $B_S = \left\lfloor \frac{N}{N_S} \right\rfloor$ is the number of consecutive fragments in the CPI, and $\boldsymbol{\alpha}^{(l,T_A)} = \left[\alpha_0^{(l,T_A)} \ \alpha_1^{(l,T_A)} \ \cdots \ \alpha_{K-1}^{(l,T_A)} \right]^T$ are the current filter coefficients. The latter are adaptively estimated on a longer signal fragment of duration $T_A = N_A/f_s$, symmetrically taken around the current signal fragment to be processed (see Figure 6). Basically $\boldsymbol{\alpha}^{(l,T_A)}$ are evaluated as

$$\boldsymbol{\alpha}^{(l,T_A)} = \left[\mathbf{S}_r^{(l,T_A)^H} \mathbf{S}_r^{(l,T_A)} \right]^{-1} \mathbf{S}_r^{(l,T_A)^H} \mathbf{s}_s^{(l,T_A)} \quad (19)$$

where the surveillance vector is given by

$$\mathbf{s}_s^{(l,T_A)} = \left[s_s \left[lN_S + \frac{N_S - N_A}{2} \right], s_s \left[lN_S + \frac{N_S - N_A}{2} + 1 \right], \right.$$

$$\cdots, s_s\left[lN_S + \frac{N_S + N_A}{2} - 1\right]\Big]^T \quad (N_A \times 1) \tag{20}$$

and $\mathbf{S}_r^{(l,T_A)}$ is a $N_A \times K$ matrix collecting the delayed copies of the corresponding reference signal fragment of duration T_A. Obviously, with the ECA-B approach we have $T_B = T_S = T_A$.

Based on the ECA-S cancellation algorithm, the theoretical derivation in Section III can be repeated under the same simplifying hypotheses. To this purpose, let us collect in vectors $\mathbf{s}_s^{(l,Ts)}$ and $\mathbf{s}_r^{(l,Ts)}$ the N_S samples of the *l*-th fragment of the surveillance and the reference signals, respectively:

$$\mathbf{s}_{s/r}^{(l,Ts)} = \left[s_{s/r}[lN_S],\ s_{s/r}[lN_S + 1], \cdots, s_{s/r}[(l+1)N_S - 1]\right]^T \quad (N_S \times 1) \tag{21}$$

These vectors include the N_S samples that are processed using the same filter weights according to (18). Therefore, eq. (18) can be written in matrix notation as

$$\mathbf{s}_{ECA-S}^{(l,Ts)} = \mathbf{s}_s^{(l,Ts)} - \alpha_0^{(l,T_A)}\mathbf{s}_r^{(l,Ts)} \tag{22}$$

where

$$\alpha_0^{(l,T_A)} = \frac{1}{\left\|\mathbf{s}_r^{(l,T_A)}\right\|^2}\mathbf{s}_r^{(l,T_A)^H}\mathbf{s}_s^{(l,T_A)} =$$

$$\frac{1}{|A_r|^2\|\mathbf{d}^{(l,T_A)}\|^2}\left[A_r^* A_t \mathbf{d}^{(l,T_A)^H}\mathbf{d}_{f_d}^{(l,T_A)} + A_r^* A_c\left\|\mathbf{d}^{(l,T_A)}\right\|^2 + \right.$$

$$\left. + A_r^* \mathbf{d}^{(l,T_A)^H}\mathbf{w}_s{}^{(l,T_A)}\right] \tag{23}$$

being $\mathbf{d}^{(l,T_A)}$ and $\mathbf{d}_{f_d}^{(l,T_A)}$ the $N_A \times 1$ vectors containing the *l*-th overlapped batch of duration T_A of the direct signal and its Doppler shifted version.

Therefore, proceeding as in (8)-(9), we evaluate the output of the range-Doppler map for the range bin of the target at the generic Doppler frequency f_0:

$$\bar{\chi}[f_0] = \sum_{l=0}^{B_S-1} A_t \mathbf{d}_{f_0}^{(l,Ts)^H}\mathbf{d}_{f_d}^{(l,Ts)} +$$

$$- \sum_{l=0}^{B_S-1} \frac{A_t}{\|\mathbf{d}^{(l,T_A)}\|^2}\mathbf{d}^{(l,T_A)^H}\mathbf{d}_{f_d}^{(l,T_A)}\mathbf{d}_{f_0}^{(l,Ts)^H}\mathbf{d}^{(l,Ts)} +$$

$$+ \sum_{l=0}^{B_S-1}\left[\mathbf{d}_{f_0}^{(l,Ts)^H}\mathbf{w}_s{}^{(l,Ts)} + \right.$$

$$\left. - \frac{1}{\|\mathbf{d}^{(l,T_A)}\|^2}\mathbf{d}_{f_0}^{(l,Ts)^H}\mathbf{d}^{(l,Ts)}\mathbf{d}^{(l,T_A)^H}\mathbf{w}_s{}^{(l,T_A)}\right] \tag{24}$$

Again, the first target contribution in (24) results:

$$\bar{\chi}_I[f_0] = A_t \frac{sin[\pi(f_d - f_0)\,N/f_s]}{sin[\pi(f_d - f_0)/f_s]} e^{j\pi(f_d - f_0)(N-1)/f_s} \tag{25}$$

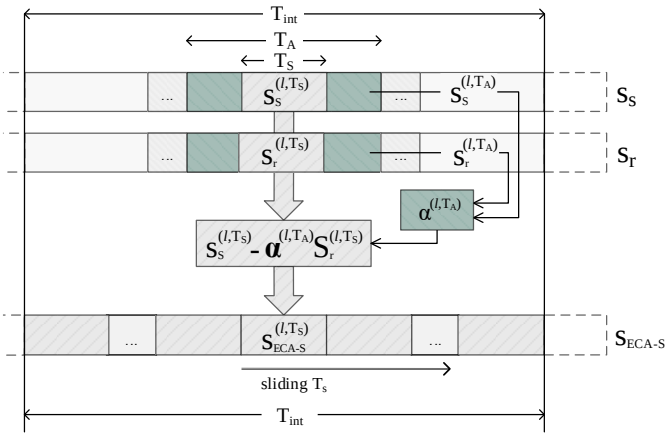

Figure 6. Block diagram of ECA-S.

This coincides with eq. (11) since this term represents the ideal target contribution at the output of the 2D-CCF and it is not affected by the cancellation stage.

The second term in eq. (24) can be written as:

$$\bar{\chi}_{II}[f_0] =$$

$$= A_t N_A N_S \sum_{l=0}^{B_S-1} \frac{1}{\|\boldsymbol{d}^{(l,T_A)}\|^2} g^{(l,T_A)}(f_d)\left[g^{(l,Ts)}(f_0)\right]^* \tag{26}$$

where

$$g^{(l,T_A)}(f) = \mathbf{d}^{(l,T_A)^H}\mathbf{d}_f^{(l,T_A)}/N_A =$$

$$= \frac{1}{N_A}\sum_{n=lN_S+\frac{N_S-N_A}{2}}^{lN_S+\frac{N_S+N_A}{2}-1} |d[n]|^2\, e^{j2\pi f n/f_s} =$$

$$= g^{(0,T_A)}(f) e^{j2\pi f l N_S/f_s} \tag{27}$$

and

$$g^{(l,Ts)}(f) = \mathbf{d}^{(l,Ts)^H}\mathbf{d}_f^{(l,Ts)}/N_S =$$

$$= \frac{1}{N_S}\sum_{n=lN_S}^{(l+1)N_S-1} |d[n]|^2\, e^{j2\pi f n/f_s} =$$

$$= g^{(0,Ts)}(f) e^{j2\pi f l N_S/f_s} \tag{28}$$

being

$$g^{(0,T_A)}(f) = \frac{1}{N_A}\frac{sin[\pi f N_A/f_s]}{sin[\pi f/f_s]} e^{j\pi f(N_S-1)/f_s} \tag{29}$$

and

$$g^{(0,Ts)}(f) = \frac{1}{N_S}\frac{sin[\pi f N_S/f_s]}{sin[\pi f/f_s]} e^{j\pi f(N_S-1)/f_s} \tag{30}$$

Therefore eq. (26) becomes:

$$\bar{\chi}_{II}[f_0] = A_t N_S g^{(0,T_A)}(f_d)\left[g^{(0,T_S)}(f_0)\right]^* \cdot$$

$$\cdot \frac{sin[\pi(f_d - f_0)\, B_S N_S/f_s]}{sin[\pi(f_d - f_0)\, N_S/f_s]} e^{j\pi(f_d - f_0)\, N_S(B_S-1)/f_s} \quad (31)$$

As is apparent, this term still include a $\sin(B_S x)/\sin(x)$ factor; however in this case the period is set by the filter update rate. In other words, operating with the ECA-S approach, the Doppler ambiguities associated to low Doppler targets are expected to appear with Doppler separation equal to $\frac{f_s}{N_S} = \frac{1}{T_S}$. Therefore, a reasonable strategy to design this parameter is to select T_S so that to move out of the Doppler range of interest $[-f_{Dmax}, f_{Dmax}]$ the undesired structures arising from the batch processing of the received signals. By imposing this condition for all the targets belonging to the cancellation notch area, we obtain $T_S < \left(f_{Dmax} + \frac{1}{2T_A}\right)^{-1}$. A good cancellation capability can be still guaranteed by acting on the other independent parameter T_A. Specifically this can be selected according to the analysis reported in Section II, in order to allow remarkable cancellation performance against the time-varying characteristics of the disturbance for the specific operative scenario; obviously, this should be partly traded with the minimum detectable velocity to be guaranteed.

In fact the target peak amplitude (i.e. for $f_0 = f_d$) at the output of the 2D-CCF can be evaluated in this case as:

$$\bar{\chi}[f_d] = \bar{\chi}_I[f_d] - \bar{\chi}_{II}[f_d] =$$

$$= A_t N \left\{1 - \frac{1}{N_S N_A} \frac{sin[\pi f_d N_S/f_s]}{sin[\pi f_d/f_s]} \frac{sin[\pi f_d N_A/f_s]}{sin[\pi f_d/f_s]}\right\} \quad (32)$$

As is apparent, the target SNR loss, and in turn, the cancellation notch width, depends on both T_A and T_S.

Notice that if the ECA-B operates with $T_B = T_S$ aiming at excluding the ambiguities from the observed Doppler region, a wide cancellation notch could be achieved; in contrast the ECA-S yields the possibility to significantly narrow the cancellation notch by properly selecting $T_A > T_S$.

However, when the batch duration of the ECA-B is selected as $T_B = T_A$ to maximize the cancellation capability, the ECA-S typically yields a wider Doppler extent of the cancellation area with respect to the ECA-B since the T_S value required to remove Doppler ambiguities is much smaller than T_A (see eqs. (32) and (16)). In other words, operating with the ECA-S allows to trade the ambiguities removal with a limited SNR loss. In turn, the latter can be traded with a small cancellation loss if T_A is slighly increased with respect to the initial choice $T_A = T_B$.

Based on the considerations above, we here address the design of the ECA-S parameters with reference to the different case studies considered in this paper (see Sections II.A, II.B, and II.C).

When the FM-based PCL is employed for ATC applications, the batch duration exploited to estimate the filter coefficients can be selected as $T_A = 25$ ms which was experimentally verified to yield remarkable and quite stable cancellation performance in the considered scenario (see Figure *1*). In contrast, assuming a maximum velocity $v_{max} = 400$ m/s ($f_{Dmax} = 126$ Hz with the exploited FM radio channel at 94.5 MHz), we might set $T_S < 6.8$ ms.

In the case of a DVB-T based PCL for maritime surveillance, again the batch duration T_A can be independently set to maximize the cancellation performance: for example $T_A = 0.1$ s is a reasonable choice according to the analysis in Section II.B. Furthermore, the maximum observed velocity can be limited to $v_{max} = 20$ m/s so that $T_S < 17.4$ ms allows to set the first Doppler ambiguity out of the observed area in our case studies ($f_{Dmax} < 52.4$ Hz with the DVB-T channels exploited in the considered data sets).

Finally, in the WiFi-based PCL case, a batch duration $T_A = 50$ ms has been shown to be a good compromise for effective disturbance removal and reasonable target echo preservation. Moreover, as the maximum Doppler frequency observed is $f_{Dmax} = 70$ Hz, we might set $T_S < 12.5$ ms.

V. Performance Analysis Against Real Data

In this section, the improvement achieved by the proposed ECA-S approach is investigated in term of detection performance of the PCL system. This analysis allows us to gain a further insight into the operation of both the ECA-B and the ECA-S and to clearly demonstrate how the proposed modification recovers for the limitations identified in Section III.

We refer to the same case studies considered in Section II.

A. Experimental results for the FM-based PCL in ATC applications

Based on our experimental results [29]-[30], in this application quite long batch durations can be used normally for adaptive filter evaluation; this yields narrow cancellation notches compared to the typical high Doppler values of the aerial targets even operating with an ECA-B approach. As a consequence the adverse effects investigated in Section III occur with low probability, and, when this is the case, they appear for a very limited time thus not compromising the overall results if effective post-processing stages are implemented.

Nevertheless, we have shown that in specific condition, i.e. when operating against severe scenarios (namely those characterized by rapidly varying disturbance characteristics, possibly induced by co- and inter-channel interference, severe multipath, transmitter dependent effects, etc.) it may be necessary to operate the ECA-B with batches of extremely small dimension to effectively remove the disturbance. As a result, the undesired effects shown in the previous sections might arise limiting the surveillance capability of the PCL system.

The above considerations are experimentally verified with reference to the data set described in Section II.A. All the available data files have been processed according to a basic PCL processing scheme that includes: (i) disturbance (direct signal and multipath) cancellation using different ECA versions with K=140 taps; (ii) evaluation of the 2D-CCF between the surveillance and the reference signal over a CPI of 1 s; (iii) target detection via a cell-average constant false alarm rate (CA-CFAR) threshold with a nominal probability of false alarm P_{fa}=10^{-4}; (iv) track initiation using a conventional nearest

neighbor association scheme with a '2 out of 2' strategy. Figure 7 reports the results obtained for 100 consecutive data files.

In particular, using the conventional ECA for the disturbance removal, the results are those reported as red dots in Figure 7(a), where black dots represent the available air-truth. Due to the high non-stationarity of the environment, resorting to the ECA-B approach allows a better cancellation capability (see Section II.A) that turns out to guarantee a better continuity in target detection. As an example, the results obtained with $T_B = 25$ ms are reported in Figure 7(b). As is apparent complete plot sequences are detected and additional target tracks are correctly identified. However, it is worth noticing that operating with $T_B = 25$ ms yields a number of false tracks due to Doppler ambiguities at $1/T_B$ Hz distance from the corresponding true target track.

Figure 7(c) reports the results obtained after the disturbance removal with the ECA-S operating with $T_S = 6.25$ ms, to remove Doppler ambiguities appearing in the area of interest, and $T_A = 25$ ms, to guarantee an effective disturbance cancellation in the observed non-stationary environment. Again, a tremendous improvement is observed with respect to the conventional ECA whereas comparable detection performance is obtained with respect to the application of the ECA-B approach operating with $T_B = 25$ ms. However, the possibility to separately set the filter updating rate allows to avoid the many false tracks appearing in Figure 7(b).

B. Experimental results for the DVB-T-based PCL

As seen in Figure 2, some maritime operative scenarios may be highly time varying thus requiring the cancellation filter coefficients to be estimated over a much smaller duration than the CPI in order to adequately lower the disturbance power in the surveillance signal. Therefore, due to the low speed of many naval targets, operating with an ECA-B approach might yield the limitations discussed in Section III.

This is shown in Figure 8 with reference to the data sets mentioned in Section II.B. All the available data files have been fed into a signal processing chain composed by: (i) prefiltering of the reference signal for ambiguity function control [31]; (ii) disturbance cancellation using different ECA versions with $K = 1000$ taps; (iii) evaluation of the 2D-CCF between the surveillance and the reference signal over a CPI of 1 s; (iv) target detection via a CA-CFAR threshold with a nominal probability of false alarm P_{fa}=10^{-4}; (v) '2 out of 2' criterion to integrate the detection obtained at the 2 available surveillance channels; (vi) track initiation stage using a conventional nearest neighbor association scheme with a '2 out of 2' strategy.

Figure 8 reports the comparison of the results obtained over 90 consecutive data files of Data Set 1 after cancellation with ECA-B and ECA-S. Red dots represent PCL detections while blue tracks represent the ground truth provided by AIS. As is apparent, ECA-B operating with $T_B = 0.1$ s (see Figure 8(a)) gives rise to several false tracks that may prevent a proper awareness of the number of vessels in the surveilled zone. They are spaced in the bistatic Doppler dimension at $1/T_B$ Hz that results in 6.22 m/s spacing in the bistatic velocity domain (at the considered carrier frequency). Figure 8(b) shows the results for disturbance removal with ECA-S operating with $T_A = 0.1$ s and $T_S = 15$ ms. As is apparent the proposed approach allows the complete removal of the false tracks appearing between 24 and 30 km; detections wrapped in the dotted ellipse have been attributed to an interfering transmitter and have been verified to be revealed also after cancellation via conventional ECA. Plot sequences at 7-15 km and at 16-20 km are likely to be traffic of opportunity not equipped with AIS.

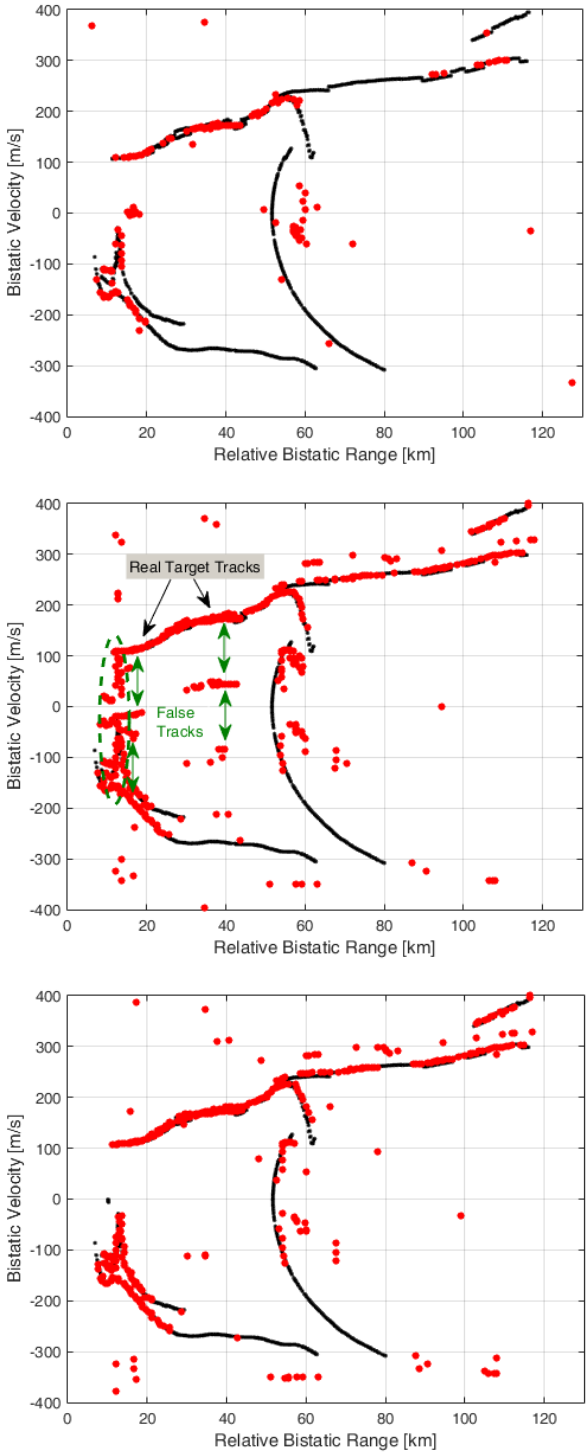

Figure 7. Detection results over the bistatic range-velocity plane for 100 consecutive scans when disturbance removal is performed via: (a) the conventional ECA; (b) the ECA-B with $T_B = 25$ ms; (c) the ECA-S with $T_A = 25$ ms and $T_S = 6.25$ ms.

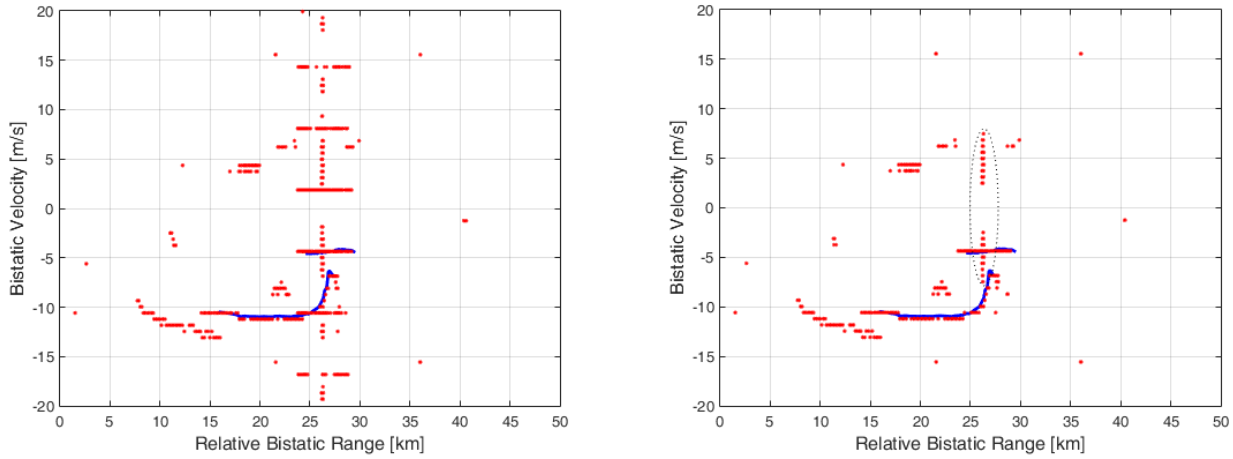

Figure 8. Detection results over the bistatic range-velocity plan for 90 consecutive data files of Data Set 1 with disturbance removal performed via: (a) ECA-B with $T_B = 0.1$ s; (b) ECA-S with $T_A = 0.1$ s and $T_S = 15$ ms

Based on other similar analyses, we might conclude that the ECA-S yields similar cancellation performance with respect to the previous batch version of the ECA, and this results in a comparable capability of detecting real target tracks. Furthermore, the ECA-S allows to recover for the limitations of the ECA-B arising when operating against slowly moving targets so that it can be regarded as a better solution for disturbance removal also in this application.

Therefore, in the following we focus on the comparison of ECA-S with the conventional ECA aiming at understanding the benefits deriving from a batch approach in different maritime scenarios.

To this purpose Figure 9 reports some examples of detection results obtained at different acquisitions; specifically, in each figure, an enlarged view is shown around specific targets of opportunity. Figure 9(a-b) reports the detections over 90 data files for a cargo ship observed in Data Set 1 at very long bistatic range (>200 km); Figure 9(a) is obtained after the application of ECA while Figure 9(b) reports the results of ECA-S. We recall that Data Set 1 was collected in a quite stationary scenario so that the performance yield by the two approaches are very similar, even though a slight better continuity is obtained when operating with ECA-S.

Figure 9(c-d) report the results over 66 data files of Data Set 6 which accounts for a highly varying disturbance scenario. In this case tremendous advantage offered by ECA-S is quite apparent since it allows to significantly improve the detection rate for the considered 22 m sailing vessel at medium ranges.

The number of correct detections obtained with the ECA and the ECA-S in the above examples has been reported in Table I (first and last line) along with other examples from the available data sets. In each case we indicate the considered Data Set and provide details about the target of opportunity (name, type, size, bistatic range-velocity coordinates). The number of correct detections obtained after ECA and ECA-S are compared to the total number of available data files. Cancellation via ECA provides very similar detection performance with respect to ECA-S when the system operates in a quasi stationary scenario (see results obtained for Data Set 1). Remarkable detection rates could be obtained after the ECA even in non-stationary scenarios (i.e. Data Sets 3-6); however, in this case, the size of

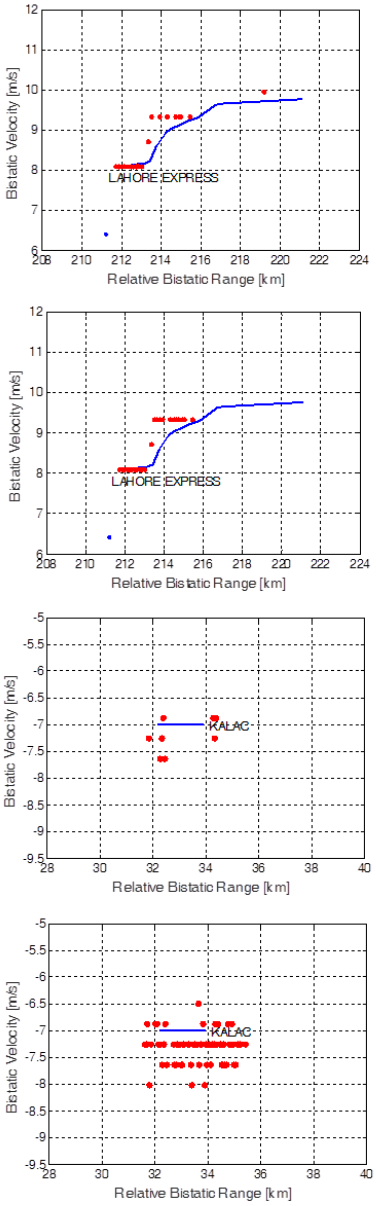

Figure 9. Comparison of detection results with ECA and ECA-S for specific targets of opportunity: (a-b) Cargo ship detected in Data Set 1 operating with ECA and ECA-S, (c-d) Sailing vessel detected in Data Set 6 operating with ECA and ECA-S.

Table I. Detection results comparison against various targets of opportunity in different acquisitions.

Data set	Target	Type	Size [m]	Bistatic range [km]	Bistatic velocity [m/s]	Available scans	Associated detection	
							ECA	ECA-S
1	Lahore Express	Cargo	259x32	213	9	90	25	27
1	Besiktas GH	Tanker	123x19	140	-12,5	90	77	79
3	Vastaso	Tanker	176x31	17	1	42	42	42
3	Camilla	Container	184x25	16	-4	42	15	19
3	SS Trinità	Fishing	26x6	12,5	-1,5	42	8	12
4	Alida S	Cargo	116x16	37	7,5	43	2	41
5	Alida S	Cargo	116x16	29	6	45	32	43
5	Nuovo Ciclone	Fishing	22x6	34	-3	45	0	16
6	Kalac	Sailing	14x5	33	-7	66	11	61

the target and its distance from the receiver play an important role to ensure the same performance. In fact, a comparable detection continuity is observed for big-sized targets at short/medium ranges. In contrast, ECA-S dramatically increase the number of correct detections against small targets such as fishing or sailing vessels (see for example targets Nuovo Ciclone and Kalac).

C. Experimental results for the WiFi-based PCL

The effectiveness of the sliding version of the ECA is further demonstrated in this sub-section for WiFi-based PCL. Specifically Figure 10 shows the detection results obtained with ECA and ECA-S for the same data set considered in Section III (test against a vehicular target moving in the cross-range direction).

The data collected has been processed according to the WiFi-based passive radar processing scheme presented in [34]. In particular, the cancellation stage is performed by adopting the ECA-B or the ECA-S over a range of 500 m. A CPI of 0.2 s is then used to evaluate the bistatic range-velocity map over consecutive portions of the acquired signals (frames) with a fixed displacement of 0.1 s (10 frames per second are thus obtained); finally, target detection is performed by resorting to a standard cell-average CFAR threshold with a probability of false alarm equal to 10^{-5}.

In Figure 10 we report the raw detections over the bistatic range/velocity plane collected along the whole acquisition (20 seconds). Specifically Figure 10(a) has been obtained after cancellation via ECA-B operating with $T_B = 50$ ms while Figure 10(b) is the result of the application of the ECA-S. Notice that for ECA-S, the adopted parameters are $T_A = 50$ ms and $T_S = 3$ ms; in fact, for a practical application, we set the filter update rate to be equal to the beacon emission rate of the exploited access point, i.e. the filter coefficients are updated beacon by beacon.

As is apparent, in both figures, in addition to the target returns (the cross-range movement of the target results in a parabolic sequence of detections over the range/velocity plane with vertex in (40;0)), there are also the double bounce returns caused by the reflection of the target echo over the metallic fence delimiting the parking area (parabolic sequence with vertex in (140;0)) and false alarms.

In addition, operating with the ECA-B yields a number of false plots due to Doppler ambiguities with 2.3 m/s spacing (corresponding to $1/T_B$ = 20 Hz). These ambiguities arise both from the main target echo and from its double-bounce return; however they are more evident in the first case due to the higher SNR of the originating echo. False tracks are usually discontinuous thanks to the masking effect of the real target echo at the detection stage. Nevertheless they are quite apparent and might significantly limit the capability to identify and effectively track the true targets.

In contrast, we observe that the ECA-S allows to move the Doppler ambiguities out of the Doppler extent of interest while guaranteeing largely comparable detection capability against the true target echoes.

VI. CONSIDERATIONS ON THE COMPUTATIONAL COST

The advantages yield by the ECA-S are paid in terms of computational load since the filter weights computation is repeated a greater number of times within the CPI with respect to both the ECA and the ECA-B. However we show that the required computations can be limited if proper expedients are adopted.

Based on eqs. (1)-(2), (3)-(4), and (18)-(19), the computational load of any version of the ECA can be decomposed in two main contributions:

1) the cost $C_1(K, N_x)$ required for the adaptive evaluation of the filter coefficients; this depends on the number of taps and on the length of the signal fragment used for adaptive weights estimation (namely, $N_x = N$ for ECA, $N_x = N_B$ for ECA-B, and $N_x = N_A$ for ECA-S).
2) The cost $C_2(K, N_y)$ required for the application of the filter to the surveillance signal; this again depends on K and on the length of the signal fragment processed with a given filter estimate (namely, $N_y = N_x$ for ECA and ECA-B, whereas $N_y = N_S$ for ECA-S).

Therefore the computational load for ECA is simply

$$C_{ECA}(K, N) = C_1(K, N) + C_2(K, N) \tag{33}$$

In contrast, when operating with the ECA-B and ECA-S approaches, the two tasks above are performed against smaller signal fragments but they are repeated at each considered, possibly overlapped, batch, i.e.

$$C_{ECA-B}(K, N_B) = B\,[C_1(K, N_B) + C_2(K, N_B)] \tag{34}$$

$$C_{ECA-S}(K, N_A, N_S) = B_S\,[C_1(K, N_A) + C_2(K, N_S)] \tag{35}$$

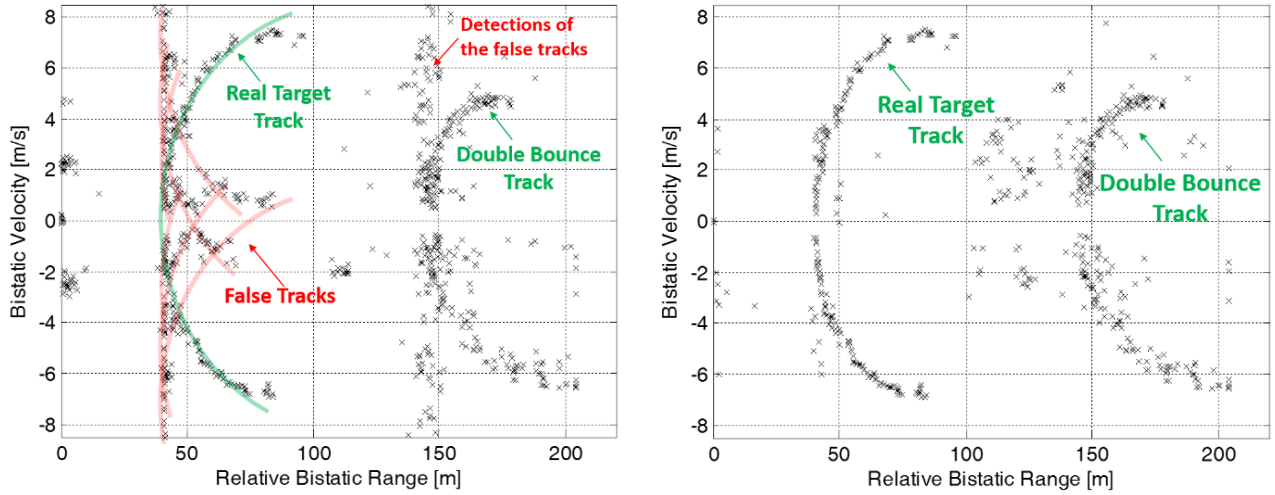

Figure 10. Detection results over the bistatic range-velocity plane when disturbance removal is performed via: (a) the ECA-B with $T_B = 50$ ms; (b) the ECA-S with $T_A = 50$ ms and $T_S = 3$ ms.

Notice that the direct implementation of eqs. (2), (4), and (19), requires $C_1(K, N_x) = O[4N_x K^2 + 4K^3]$ FLOPs (FLoating-point Operations; here we assume that a complex add involves 2 FLOPs and a complex multiplication involves 6 FLOPs). The filter application is much less computationally expensive since it requires $C_2(K, N_y) = 8\mathrm{N_y K}$ FLOPs with $N_y \leq N_x$. Therefore $C_1(K, N_x)$ drives the final cost of the cancellation stage and, depending on the values of the relevant parameters, the number of required FLOPs could rapidly increase so that this stage might become the bottleneck for a real-time operation. This especially applies to the ECA-S approach where the filter computation is repeated many times along the CPI (we recall that in all the considered applications $B_S > B$ and $N_A \geq N_B$).

As is apparent, appropriate expedients should be devised to limit the computational load of the adaptive filter evaluation with respect to the direct implementation of eqs. (2), (4), and (19).

To this purpose, let us rewrite eq. (2) as

$$\boldsymbol{\alpha} = \mathbf{M}^{-1}\mathbf{c} \tag{36}$$

where $\mathbf{M} = \mathbf{S}_r^{\mathrm{H}}\mathbf{S}_r$ and $\mathbf{c} = \mathbf{S}_r^{\mathrm{H}}\mathbf{s}_s$. The following considerations identically apply to other ECA approaches with an obvious change of notation. Based on the definition of matrix $\mathbf{S}_r$, the k-th element of vector $\mathbf{c}$ can be evaluated as:

$$c[k] = \sum_{n=0}^{N-1} s_r^H[n-k]s_s[n] \quad k = 0,..,K-1 \tag{37}$$

Notice that it coincides with the k-th sample of the cross-correlation between the reference and the surveillance signals. Therefore the whole vector $\mathbf{c}$ can be computed at FFT speed by performing the FFT of $\boldsymbol{s}_s$ and $\boldsymbol{s}_r$, evaluating the IFFT of their conjugate product, and then selecting the useful samples.

Similarly, the $[k,l]$-th element of matrix $\mathbf{M}$ can be rewritten as:

$$M[k,l] = \sum_{n=0}^{N-1} s_r^H[n-k]s_r[n-l] \cong m[k-l]$$
$$k,l = 0,..,K-1 \tag{38}$$

where, for the last equality, we neglect the border effect or, equivalently, we assume that the reference signal is locally stationary so that its autocorrelation depends only on the time-distance between delayed replicas. Apparently this approximation is largely acceptable when $K \ll N$, as for typical applications. In addition we observe that $m[k] = m^*[-k]$. Therefore we conclude that $\mathbf{M}$ is an Hermitian positive definite Toeplitz matrix so that it is completely defined by its first row (or column). Consequently, matrix $\mathbf{M}$ can be computed using the same approach adopted for vector $\mathbf{c}$, by exploiting the FFT of $\boldsymbol{s}_r$ available from the previous step. Overall, the computation of $\mathbf{M}$ and $\mathbf{c}$ requires $17.5N\log_2(N) + 8.5N$.

Once the required matrices have been computed, the direct implementation of (36) would require the inversion of a $K \times K$ matrix. To limit the corresponding computational load, we might observe that vector $\boldsymbol{\alpha}$ is the solution of an Hermitian positive definite Toeplitz system $\mathbf{M}\boldsymbol{\alpha} = \mathbf{c}$. This can be efficiently solved by resorting to the Levinson algorithm which requires approximately $16K^2$ FLOPs [38]. Therefore, for a typical number K of taps, a significant computational load can be saved with respect to the $O(4K^3)$ complexity of conventional matrix inversion.

Therefore, generalizing the result to different versions of the ECA, the number of FLOPs required for the adaptive filter evaluation has been reduced down to $C_1(K, N_x) = 17.5N_x\log_2(N_x) + 8.5N_x + 16K^2$ FLOPs.

Similar expedients can be adopted to further limit the computational load required for filter application. To this purpose eq. (1) is rewritten as $s_{ECA}[n] = s_s[n] - y[n]$ where

$$y[n] = \sum_{k=0}^{K-1} \alpha_k s_r[n-k] \quad n = 0,\ldots,N-1 \tag{39}$$

Table II. Number of FLOPs required for the efficient implementation of different ECA versions.

ECA Version	Number of FLOPs
ECA	$C_{ECA}(K,N) = 27.5N\log_2(N) + 16.5N + 16K^2$
ECA-B	$C_{ECA-B}(K,N_B) = B\,[27.5N_B\log_2(N_B) + 16.5N_B + 16K^2]$
ECA-S	$C_{ECA-S}(K,N_A,N_S) = B_S\,[17.5N_A\log_2(N_A) + 15N_S\log_2(N_S) + 16K^2 + 8.5N_A + 8N_S]$

is the output of the convolution between the reference signal and the filter. Again, this can be evaluated in the frequency domain by performing the FFT of $\boldsymbol{s}_r$ and the zero-padded version of $\boldsymbol{\alpha}$, and then evaluating the IFFT of their product. Therefore, for the generic ECA version, the computation of the output with given filter coefficients requires $C_2(K,N_y) = 15N_y\log_2(N_y) + 8N_y$ FLOPs. Notice that if $N_y = N_x$ (as for ECA and ECA-B), the FFT of the reference signal fragment to be processed is available from the previous step so that $C_2(K,N_y)$ can be further reduced down to $C_2(K,N_y) = 10N_y\log_2(N_y) + 8N_y$ FLOPs.

The overall complexity of the different ECA versions is reported in Table II.

As is apparent, for typical values of the relevant parameters, the ECA-S is still the most demanding approach in term of computational load. However, its complexity has been significantly reduced with respect to the direct implementation of eqs. (18)-(19). In many cases, such reduction might enable a real-time operation or, at least, remove the cancellation stage from the role of bottleneck of the PCL processing chain.

This is shown in Figure 11 where the complexity of the different ECA versions is compared to the number of FLOPs required for the evaluation of a Range-Doppler map according to an efficient optimum algorithm. Specifically we refer to the case of DVB-T based PCL for maritime surveillance application as it represents the most demanding application in term of computational burden. Specifically we consider the Correlation-FFT algorithm for the 2D-CCF evaluation since it represents the most efficient solution when DVB-T transmissions are exploited [33]. The corresponding computational load is reported in [33] and is essentially determined by the number of integrated samples N and the number N_f of Doppler bins included in the range-Doppler map.

The results in Figure 11 are shown as a function of the CPI. As expected, the number of FLOPs required for ECA-S is higher than for ECA and ECA-B; this is indeed the price to be paid to obtain the observed performance improvement (see Section V.B for this specific application). However we observe that the increase in complexity is asymptotically constant and smaller than an order of magnitude.

Nevertheless, it is to be noted that the computational load required by ECA-S is much lower than that required for 2D-CCF evaluation for typical values of the CPI (i.e. CPI>1 s for this application) and the gap widens as the CPI increases. The Range-Doppler map computation is indeed a key step of the PCL signal processing. Therefore the analysis above clearly

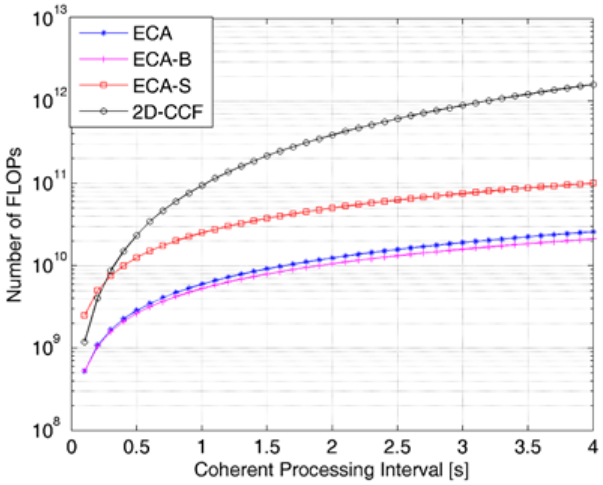

Figure 11. Number of FLOPs as a function of the CPI for the different ECA versions in comparison with the 2D-CCF evaluation in the case of DVB-T application.

shows that, despite the increased complexity with respect to previous ECA versions, the proposed ECA-S approach does not represent the bottleneck in the PCL signal processing chain.

As a last remark, from both Table II and Figure 11, we observe that the ECA and the ECA-B approaches largely benefit from the proposed efficient implementation. In this regard, the discussion reported in this section gains a more general value as the expedients introduced above can be fruitfully adopted to limit also the computational burden of the previous ECA versions. This makes these previous versions more appealing, at least for those applications that do not imply the limitations discussed in this paper.

VII. Conclusion

In this paper, a modified version of the ECA-Batches has been presented to cope with some limitations observed when dealing with highly varying disturbance characteristics in the presence of slowly-moving targets or targets moving mainly along the cross-range direction. This ECA-Sliding approach operates on partially overlapped portions of the received signals so that it takes advantage of a smooth estimate of the filter coefficients.

The effectiveness of the proposed approach has been verified with reference to several live data sets accounting for very different PCL applications. The experimental results show that the ECA-S approach allows a better trade-off between disturbance cancellation and the capability to preserve low-

Doppler target echoes thus improving the detection performance of the resulting PCL system. Following the discussion on its efficient implementation, the proposed ECA-S can be regarded as an effective solution for practical PCL applications.

ACKNOWLEDGMENT

The authors gratefully acknowledge the collaboration of Dr. A. Macera and Dr. C. Bongioanni in setting up the experimental prototypes and the acquisition campaigns for the passive radar based on FM radio and WiFi transmissions.

The work on WiFi-based passive radar has been carried out under the support of the European Project FP7-PEOPLE-2011-IAPP: SOS - "Sensors system for detection and tracking Of dangerous materials in order to increase the airport Security in the indoor landside area".

REFERENCES

[1] A. Farina and H. Kuschel, Special Issue on Passive Radar (Part I&II) – *IEEE Aerospace and Electronic Systems Magazine*, vol. 27, no. 10-11, 2012.

[2] P. Howland, Special Issue on Passive Radar Systems – *IEE Proceedings on Radar, Sonar and Navigation*, vol.152, no. 3, June 2005.

[3] A. Farina and M. Lesturgie, Special issue on Bistatic and MIMO radars and their applications in surveillance and remote sensing – *IET Radar, Sonar & Navigation*, vol. 8, no. 2, 2014.

[4] C. Zhou, J. D. Sahr, M. G. Meyer, and D. M. Gidner, "Ground clutter subtraction algorithm for VHF passive radar observation of the upper atmosphere," URSI 2002, Maastrict, Aug. 2002.

[5] A. Guner, M.A. Temple, and R.J. Claypoole, Jr., "Direct-path filtering of DAB waveform from PCL receiver target channel," *Electronic Letters*, vol. 39, no. 1, 2003.

[6] S.R.J. Axelsson, "Improved clutter suppression in random noise radar," URSI 2005 Commission F Symposium on Microwave Remote Sensing of the Earth, Oceans, Ice, and Atmosphere, April 2005.

[7] P.E. Howland, D. Maksimiuk, and G. Reitsma, "FM radio based bistatic radar," *IEE Proc. on Radar, Sonar and Navigation*, vol. 152, no. 3, June 2005.

[8] D. Poullin, "Passive detection using digital broadcasters (DAB, DVB) with COFDM modulation," *IEE Proc. on Radar, Sonar and Navigation*, vol. 152, no. 3, June 2005.

[9] K. Kulpa and Z. Czekala, "Masking effect and its removal in PCL radar," *IEE Proc. on Radar, Sonar and Navigation*, vol. 152, no. 3, June 2005.

[10] D.W. O'Hagan, C.J. Baker, and H.D. Griffiths, "Signal and Interference Analysis: Proposed Analogue Signal Suppression Techniques for PCL Radar," *3rd European Radar Conference, EuRAD 2006*, Sept. 2006.

[11] Wan Hong, Li Shentang, and Wang Zhigang, "Direct Path Interference Cancellation in FM Radio-Based Passive Radar," *8th Int. Conf. on Signal Processing*, vol.1, 2006.

[12] R. Cardinali, F. Colone, C. Ferretti, and P. Lombardo, "Comparison of clutter and multipath cancellation techniques for passive radar," *IEEE Radar Conference 2007*, Boston, Massachusetts, USA, April 2007.

[13] F. Colone, D. W. O'Hagan, P. Lombardo, and C. J. Baker, "A multistage processing algorithm for disturbance removal and target detection in Passive Bistatic Radar," *IEEE Transactions on Aerospace and Electronic Systems*, vol. 45, no. 2, April 2009.

[14] J.E. Palmer and S.J. Searle, "Evaluation of adaptive filter algorithms for clutter cancellation in Passive Bistatic Radar," *IEEE Radar Conference 2012*, Atlanta, May 2012.

[15] M. Meller, "Processing of noise radar waveforms using block least mean squares algorithm," *IEEE Trans. Aerosp. Electron. Syst.*, vol. 48, no. 1, 2012.

[16] Y.D. Zhao, Y.K. Zhao, X.D. Lu, and M.S. Xiang, "Block NLMS cancellation algorithm and its real-time implementation for passive radar," *IET International Radar Conference 2013*, April 2013.

[17] B. Demissie, "Clutter cancellation in passive radar using GSM broadcast channels," *IET Radar, Sonar & Navigation*, vol. 8, no.7, Aug. 2014.

[18] Guan Xin, Hu Dong-hui, Zhong Li-hua, and Ding Chi-biao, "Strong Echo Cancellation Based on Adaptive Block Notch Filter in Passive Radar," *IEEE Geoscience and Remote Sensing Letters*, vol. 12, no. 2, Feb. 2015.

[19] Z. Zhao, X. Wan, Q. Shao, Z. Gong, and F. Cheng, "Multipath clutter rejection for digital radio mondiale-based HF passive bistatic radar with OFDM waveform," *IET Radar, Sonar & Navigation*, vol. 6, no. 9, Dec. 2012.

[20] M. John, M. Inggs, and D. Petri, "Real time processing of networked passive coherent location radar system," International Journal of Electronics and Telecommunications, vol. 57, no. 3, 2011.

[21] M.R. Inggs and C.A. Tong, "Commensal radar using separated reference and surveillance channel configuration", *Electronics Letters*, vol. 48, no. 18, 2012.

[22] H.-W. Li and J. Wang, "Particle filter for manoeuvring target tracking via passive radar measurements with glint noise," *IET Radar, Sonar and Navigation*, vol. 6, no. 3, 2012.

[23] Zhixin Zhao, Xianrong Wan, Delei Zhang, and Feng Cheng, "An Experimental Study of HF Passive Bistatic Radar Via Hybrid Sky-Surface Wave Mode," *IEEE Transactions on Antennas and Propagation*, vol. 61, no. 1, Jan. 2013.

[24] D.K.P. Tan, M. Lesturgie, H. Sun, and Y. Lu, "Space–time interference analysis and suppression for airborne passive radar using transmissions of opportunity," *IET Radar, Sonar & Navigation*, vol. 8, no. 2, Feb. 2014.

[25] L. Xiao-Yong, W. Jun, and W. Jue, "Robust direction of arrival estimate method in FM-based passive bistatic radar with a four-element Adcock antenna array," I*ET Radar, Sonar and Navigation*, vol. 9, no. 4, 2015.

[26] H. Wang, J. Wang, and L. Zhong, "Mismatched filter for analogue TV-based passive bistatic radar," *IET Radar, Sonar and Navigation*, vol. 5, no. 5, 2011.

[27] R. Zemmari, M. Broetje, G. Battistello, and U. Nickel, "GSM passive coherent location system: Performance prediction and measurement evaluation," *IET Radar, Sonar and Navigation*, vol. 8, no. 2, 2014.

[28] J. Brown, K. Woodbridge, H. Griffiths, A. Stove, and S. Watts, "Passive bistatic radar experiments from an airborne platform," *IEEE Aerospace and Electronic Systems Magazine*, vol. 27, no. 11, 2012.

[29] F. Colone, C. Bongioanni, and P. Lombardo, "Multi-Frequency Integration in FM Radio Based Passive Bistatic Radar. Part I: Target Detection," *IEEE Aerospace and Electronic Systems Magazine*, vol. 28, no. 4, 2013.

[30] F. Colone, C. Bongioanni, and P. Lombardo, "Multi-Frequency Integration in FM Radio Based Passive Bistatic Radar. Part II: Direction of Arrival Estimation," *IEEE Aerospace and Electronic Systems Magazine*, vol. 28, no. 4, 2013.

[31] F. Colone, D. Langellotti, and P. Lombardo, "DVB-T signal ambiguity function control for passive radars," *IEEE Trans. on Aerospace and Electronic Systems*, vol.50, no.1, Jan. 2014.

[32] H. Kuschel, M. Ummenhofer, P. Lombardo, F. Colone, and C. Bongioanni, "Passive radar components of ARGUS 3D," *IEEE Aerospace and Electronic Systems Magazine*, vol. 29, no. 3, March 2014.

[33] P. Lombardo and F. Colone, "Advanced processing methods for passive bistatic radar systems," in *Principles of Modern Radar: Advanced Radar Techniques*, W. L. Melvin, and J. A. Scheer, Raleigh, NC: SciTech Publishing, 2012.

[34] F. Colone, P. Falcone, C. Bongioanni, and P. Lombardo, "WiFi-Based Passive Bistatic Radar: Data Processing Schemes and Experimental Results," *IEEE Trans. on Aerospace and Electronic Systems*, vol. 48, no. 2, April 2012.

[35] D. Pastina, F. Colone, T. Martelli, and P. Falcone, "Parasitic Exploitation of Wi-Fi Signals for Indoor Radar Surveillance," *IEEE Trans. on Vehicular Technology*, vol.64, no. 4, April 2015.

[36] D. Langellotti, F. Colone, P. Lombardo, M. Sedehi, and E. Tilli, "DVB-T based Passive Bistatic Radar for maritime surveillance," *IEEE Radar Conference 2014*, Cincinnati (OH, USA), May 2014.

[37] D. Langellotti, F. Colone, P. Lombardo, E. Tilli, M. Sedehi, and A. Farina, "Over the horizon maritime surveillance capability of DVB-T based passive radar," European Radar Conference 2014 (EuRAD 2014), Rome (Italy), October 2014.

[38] G. H. Golub and C. F. Van Loan, "Matrix Computations (3rd ed.)," Johns Hopkins University Press, Baltimore, MD, 1996.